This is a self-archived version of an original article. This version may differ from the original in pagination and typographic details.

Author(s): Romppanen, Sari; Pölönen, Ilkka; Häkkänen, Heikki; Kaski, Saara

Title: Optimization of spodumene identification by statistical approach for laser-induced breakdown spectroscopy data of lithium pegmatite ores

Year: 2023

Version: Accepted version (Final draft)

Please cite the original version:

Romppanen, S., Pölönen, I., Häkkänen, H., & Kaski, S. (2023). Optimization of spodumene identification by statistical approach for laser-induced breakdown spectroscopy data of lithium pegmatite ores. Applied Spectroscopy Reviews, 58(5), 297-317. https://doi.org/10.1080/05704928.2021.1963977

Optimization of spodumene identification by statistical approach for laser-induced breakdown spectroscopy data of lithium-pegmatite ores

Sari Romppanen[1*], Ilkka Pölönen[2], Heikki Häkkänen[3] & Saara Kaski[1]

[1] Department of Chemistry, University of Jyväskylä, P.O. Box 35, FI-40014 University of Jyväskylä, Finland

[2] Faculty of Information Technology, University of Jyväskylä, P.O. Box 35, FI-40014 University of Jyväskylä, Finland

[3] Department of Biological and Environmental Science, University of Jyväskylä, P.O. Box 35, FI-40014 University of Jyväskylä, Finland

* Corresponding author. E-mail addresses: sari.m.romppanen@jyu.fi or sari.marianne.romppanen@gmail.com (S. Romppanen), ilkka.polonen@jyu.fi (I. Pölönen), heikki.hakkanen@jyu.fi (H. Häkkänen), saara.kaski@jyu.fi (S. Kaski).

Abstract

Mapping with laser-induced breakdown spectroscopy (LIBS) can offer more than just the spatial distribution of elements: The rich spectral information also enables mineral recognition. In the presented study, statistical approaches were used for the recognition of the spodumene from lithium pegmatite ores. A broad spectral range (280–820 nm) with multiple lines was first used to establish the methods based on vertex component analysis (VCA) and K-means and DBSCAN clusterings. However, with a view to potential on-site applications, the dimensions of the data sets must be reduced in order to accomplish fast analysis. Therefore, the capability of the methods in mineral identification was tested with limited spectral range (560–815 nm) using Li-pegmatites with various mineralogical characters.

Keywords: lithium-pegmatite ore, LIBS, VCA, K-means, DBSCAN

1 Introduction

The demand for lithium has strongly increased in recent years, and in 2020 lithium was identified as critical raw material by the EU level (1). The highest proportion of the supply is currently used in battery technology (65 %), but lithium is used also in glass and ceramics (18%), lubricating greases, (5 %), polymer production (3 %), continuous casting mould flux powders (3%), and air treatment, (1 %) (2). The biggest lithium producers are Australia, Chile, China, and Argentina (2). The occurrences of lithium deposits worldwide are reviewed elsewhere, *e.g.,* (3) but in western Finland are located an economically important Kaustinen lithium pegmatite province, where the main ore mineral is spodumene (4). Theoretically spodumene contains 8.03 percent of Li_2O (5) and it is currently the most investigated and utilized Li-mineral. Coarse grain size makes beneficiation of spodumene pegmatites rather easy (3). Ore mineral composition, assemblage, grain size, and ore texture are some of the critical features need to be discovered, *e.g.*, to optimize a flotation process (6).

To exploit lithium resources more profitably, the efficiency of the whole supply chain should be enhanced. On-site information about the chemical composition and mineral distributions of samples taken during mining and beneficiation activities are crucial. Laser-induced breakdown spectroscopy (LIBS) can offer rapid chemical analysis of solid samples (7–9) and it is suitable also into analysis of mineral and rocks samples (10–12). Remotely used, LIBS is also efficient to *in situ* and real-time measurements (13). Especially handheld LIBS (12, 14, 15) has the potential to study different kinds of geological samples already in field.

The main strength of LIBS is the analysis of light elements, *e.g.*, lithium and beryllium, which is a challenge for other on-site techniques, like XRF. The use of LIBS in analysis of Li-bearing minerals has been previously reported in the literature, *e.g.*, where the focus has been in the determination of Li grades (16–18) or Li distribution (19). The known challenges in the quantitative LIBS analysis are that, firstly, the calibration should be done with samples of very similar physical and chemical matrix, *e.g.*, in Refs (16, 20). In analysis of heterogenous rock samples, finding a set of suitable reference materials may not be trivial (12). Secondly, due to the self-absorption phenomenon (21), the calibration curve built with resonance lines, which, *e.g.,* Li line 670.8 nm is known to be (22), readily shows nonlinear behavior at higher concentrations. The reported detection limits for Li-bearing minerals have been as good as 5 ppm (16, 19) and 240 ppm (18) but as discussed by Sweetapple *et al.*

(18) and Rossi *et al.* (17) the calibration of lithium needs further development. However, our aim was in developing cost-effective technique for the needs of the exploration, mining, and beneficiation industries, and instead of determining the Li grade, we focused on identification of minerals.

Each LIBS spectrum contains emission lines of the elements from the sampled area. Thus, 2D map can be constructed to visualize the locations of the selected element in a heterogeneous sample. In mineral recognition a bunch of elemental distribution maps can be misleading, because some minerals can have chemically similar composition. As seen in previous research by Sweetapple and Tassios, 2015, a Li-distribution map cannot solely explain macroscopical characters observed in the sample. Thus, our approach is to establish procedures for the characterization of spodumene. In this task, several chemometric methods, namely K-means, DBSCAN, and vertex component analysis (VCA) are used for grouping similar spectra. In this way, information of the whole LIBS spectrum is used to reveal mineralogical distributions and textures of rock samples without a priori knowledge of the sample. Development has been made for possible applications in the on-site analysis, keeping in mind that in the field the size of analyzed data must be restricted, *i.e.*, enough information must be obtained in minimal time, effort, and cost. Our suggestion is to limit the spectral information by using both narrow spectral range and pre-handling the data with principal component analyses (PCA). Therefore, the methods are first established with a data set measured at wide spectral range and then their applicability with an optimized spectral range is evaluated.

2 Material & Methods

2.1 Samples

The Kaustinen lithium pegmatite province has six known lithium deposits: Syväjärvi, Rapasaari, Länttä, Outovesi, Leviäkangas, and Emmes (4). These pegmatite rocks have comparable textures and mineralogy and can be included in albite-spodumene subgroup of lithium–cesium–tantalum (LCT) pegmatites. The main minerals include albite, quartz, spodumene, muscovite, and K-feldspar (23). Spodumene appears at the Rapasaari deposit mostly as greenish/greyish crystals, shaped like laths and these are oriented perpendicular to wall-rock contact (24). The approximate lithium concentration of spodumene at the

Rapasaari deposit was estimated as 7.21 wt% Li_2O (24). Spodumene at the Länttä deposit is similarly shaped and in addition a reddish colored form can be observed (25). The size of spodumene grains in pegmatites is typically in cm-scale, but also more fine-grained variations occur. The approximate mineral contents in the Rapasaari and Länttä deposits are presented in Table 1. Li contents in other minerals are not known, but muscovite can contain up to 3.6 % of Li_2O when lithium substitutes mostly for aluminum. Quartz can also host minor amounts of Li (26).

Table 1. The main minerals of the Kaustinen Li-pegmatite province with general formulas and approximate contents in weight-% based on previous research from the deposits of Länttä (27) and Rapasaari (24).

Mineral	Content (wt%) Rapasaari	Content (wt%) Länttä	General formula
Spodumene	14.7	16.6	$LiAlSi_2O_6$
Quartz	25.8	25.9	SiO_2
Albite	37.1	34.2	$NaAlSi_3O_8$
K-feldspar	9.5	13.1	$KAlSi_3O_8$
Muscovite	7.0	3.9	$KAl_2(AlSi_3O_{10})(OH)_2$

Four rock samples were chosen from the Länttä and Rapasaari deposits, varying in grain sizes and spodumene colors (Table 2). Spodumene grains typically exist as elongated lath shaped crystals and the samples were sawed parallel to the longest crystal axes. To verify, that orientation of mineral grains does not have significant influence on the results, another surface perpendicular to the longest spodumene axes was sawed to sample 1. In total five areas (1.5 cm × 2 cm) were mapped with LIBS. Before the LIBS measurements, photos of the analysis areas were taken both in natural light and in 248 nm light from KrF excimer laser (Lambda Physik, Optex). The macroscopic inspection of the coarse-grained samples was used to identify minerals, which was used to confirm the LIBS analysis results.

Table 2. The description of the Li-pegmatite samples.

Sample	Measurement	Sample site	Grain size	Spodumene
1	Map 1 and Map 2	Länttä	Coarse-grained	Greenish
2	Map 3	Länttä	Coarse-grained	Reddish
3	Map 4	Länttä	Medium-grained	Greenish
4	Map 5	Rapasaari	Fine-grained	Greenish / Greyish

2.2 LIBS mapping

LIBS is efficient analysis method for 2d mappings when spatial distributions are essential (28). Thus, for studying the elemental and mineralogical differences in the Li-pegmatite samples, LIBS measurements were carried out from x number of spots in y number of rows. The laser-induced plasma was generated at the excitation wavelength of 266 nm. The laser pulse duration was 3.3 ns with repetition rate 100 Hz (NT230, Ekspla). The laser energy was ~1.2 mJ (Ophir PE10-SH-V2) and the diameter of the ablated spot at the sample surface was ~135 µm. Plasma emission was collected with fused silica fiber and a long-pass filter with a cut-on of 266 nm was used in to block the laser light from the spectrometer. Maps 1 and 2 were measured at spectral range (280–820 nm) with Echelle spectrometer (Mechelle 7500, Multichannel Instruments) and ICCD (DiCAMPRO PCO). Maps 3–5 were measured at narrower spectral range (560–815 nm) using Czerny-Turner spectrometer (SP-150, Acton Research Corp.) with 300 mm-1 grating (blazed to 500 nm) and ICCD (Andor iStar). The detailed measurement parameters of the five LIBS mappings are given in Table 3.

Table 3. The specification of experiments.

Measurement parameter	Maps 1 and 2	Maps 3–5
Spectral range (nm)	280–820	560–815
Data pixels	18233	1024
Mapped area (cm)	1.5 cm × 2 cm	1.5 cm × 2 cm
Step (µm)	400	200
Sample points (row X column)	38 X 50	75 X 100
Number of acquisitions	50	10
Number of spectra	1900	7500
Delay	300 ns	50 ns
Gate	1 µs	2 µs

2.3 Statistical approaches for mineral identification

A LIBS spectrum of a certain mineral can be considered as a fingerprint within a dataset: A unique composition of emission lines with characteristic line intensity values. This enables the use of chemometric data analysis for the characterization of the LIBS spectra and an extensive review is presented elsewhere (29). In the case of mineral and rock samples several LIBS studies are published with varying techniques, *e.g.*, principal component analysis (PCA) (30–35), partial least squares (PLS) (36), partial least squares discriminant analysis (PLS-DA) (30, 34, 37–39), hybrid sparse partial least squares (SPLS) and least-squares support vector machine (LS-SVM) model (40), K-means clustering (41, 42), soft

independent modelling of class analogy (SIMCA) (35, 41), support vector machines (SVM) (39, 43), singular value decomposition (SVD) (44), convolutional neural network with two-dimensional input (2D CNN) (45), Spectral Angle Mapper (SAM) (46), and random forest (RF) (47). Our aim was to establish procedures for the characterization of spodumene with VCA, K-means, and DBSCAN without a priori knowledge of the samples. The whole statistical approach to handling the data of Maps 1–5 is presented in Fig. 1.
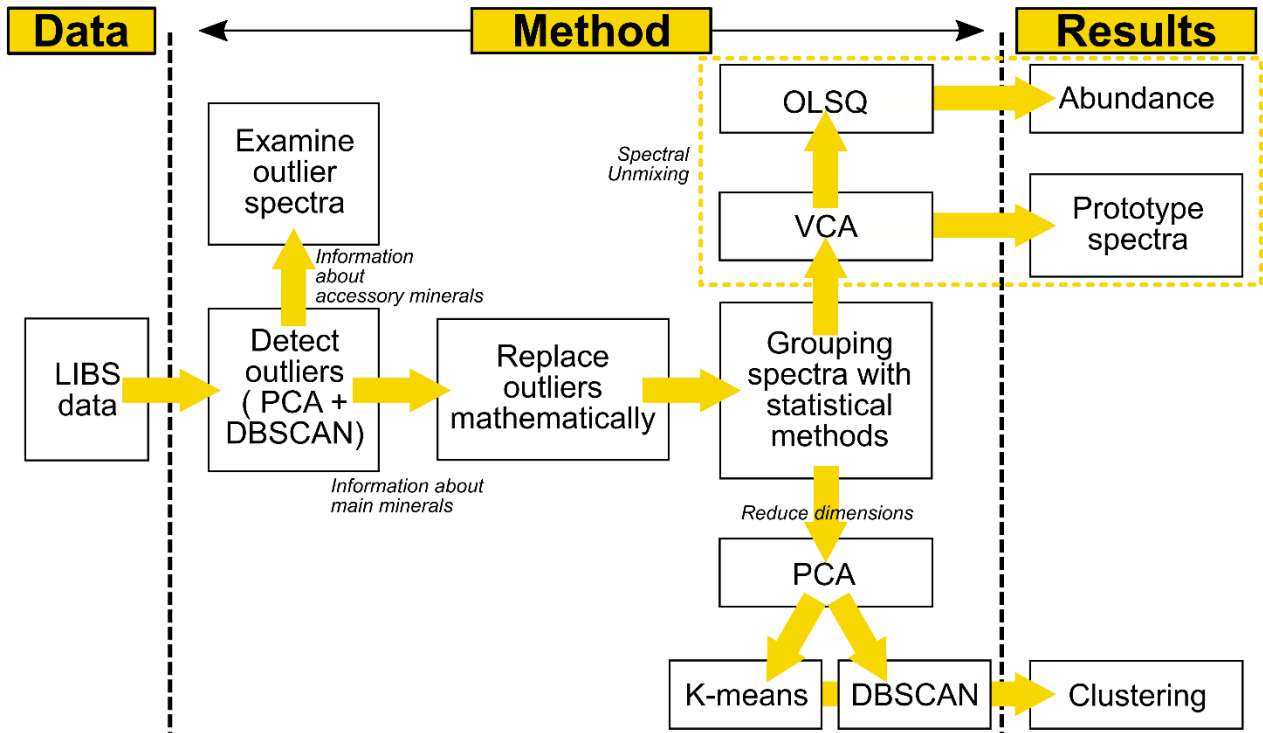

Figure. 1. Data analysis procedure for the LIBS spectra.

The principle of VCA is based on the idea, that because emission lines mostly do not overlap with each other, *i.e.*, are principally located in different parts of the spectral domain, data has strong built-in orthogonality. Mineral spectra are assumed to be a linear mixture of different elements and data itself as a linear mixture of these mineral spectra. As stated in Table 3, each spectrum of the Maps 1 and 2 consists of ~18000 pixels and therefore a single data point x is vector in $\mathbb{R}^{18000}$. This allows rearranging the spatial dataset of the measurement (row x column) to a list $X = [x_1, x_2, \ldots, x_n]^T$, where n is number of data points in the list. Now, X can be expressed as

$$X = MY,$$

where Y is matrix of prototype spectra for different minerals, $M = [\boldsymbol{m_1}, \boldsymbol{m_2}, ..., \boldsymbol{m_n}]^T$ is mixing matrix, where $\boldsymbol{m_i} = [m_1, m_2, ..., m_p]$ is a proportion of each prototype spectra for data point $\boldsymbol{x_i}$ and T is matrix transpose. It is reasonable to give non-negativity constraint for $\boldsymbol{m}$, *i.e.*,

$$m_i > 0 \; \forall \; i.$$

Often these proportions are constrained to sum to one, *i.e.*,

$$\sum_{j=1}^{p} m_j = 1$$

for each data point $\boldsymbol{x_i}$. If specific datapoint totally matches one prototype spectrum with respective mixing matrix value 1, this sample point represents the mineral given as prototype spectrum.

However, if we do not know beforehand Y, *i.e.*, have a set of mineral prototype spectra, this problem is ill-posed. Using a set of such model spectra is not trivial, because experimental variations affect relative intensities in the LIBS spectra of even pure homogeneous samples. In addition, in rock analysis a laser beam can hit more than one mineral simultaneously, especially in case of the fine-grained samples. Chemical alterations and trace element contents are also seen in a mineral LIBS spectrum. For example, in spodumene pegmatites the main Li emission is observed in almost every mineral spectrum, with at least minor intensity. Therefore, spectra are often expressed as a linear combination of two or more prototype spectra. In the latter case, the higher the value of mixing matrix is, the stronger is the contribution of that prototype spectrum in the original spectrum. VCA based spectral unmixing is a sub-pixel method, which assumes that data contains at least one pure pixel for each prototype spectrum. In this case it can show a combination of minerals in the pixel of the data set, here spectrum. Because data has strong inside orthogonality, we can use geometric approach to find Y from the data set while data points are in different parts of $\mathbb{R}^{18000}$. The data set can be covered with a convex hull. Now, the vertices of this hull are assumed to be the prototype spectra of each mineral.

To determine these vertices, here VCA (48) was used because of its computational efficiency. However, there are several other ways as well, *e.g.*, Pixel Purity Index (49). This type of data analysis is common for example in hyperspectral imaging research (50). In VCA, the data set is projected to the lower dimensional space using orthogonal projections.

Here the maximum value of the first projected component is fixed to the first prototype spectrum. Using affine transformation with this fixed component data set is rotated orthogonally and the second prototype is fixed as maximum value in this direction. This is continued until the desired number of prototype spectra is gained. Now, we know $Y = [\boldsymbol{y}_1, \boldsymbol{y}_2, \dots, \boldsymbol{y}_p]^T$, where $\boldsymbol{y}_i \in \mathbb{R}^{18000}$. Mixing matrix M can now be solved using ordinary least squares (OLSQ)

$$M = (Y^T Y)^{-1} Y^T X, \qquad\qquad [1]$$

or using non-negative least squares' algorithms. Because of the built-in orthogonality in X, equation [1] does not give negative results. Now by rearranging M to the original spatial dimensions of the imaged data we have gained relative proportion maps. These express into what extent each spectral data point can be seen as a mixture of these prototype spectra.

Cluster analysis (unsupervised machine learning) gives us information about how a data set can be divided into different clusters. In geometrical sense, clusters are data points which are near to each other. Here we are using two classical algorithms: K-means (51) and DBSCAN (52). Dimension of this LIBS data set is relatively high, each spectrum is in $\mathbb{R}^{18000}$, which makes use of distance-based algorithms computationally heavy. Thus, dimension reduction by principal component analysis (PCA) is applied to the data set before clustering. Cluster centroids express the mean value of the spectra of cluster points and can be used to explain what mineral cluster represents.

DBSCAN as a density-based algorithm is used to cluster data sets, but it is also applied in the detection of the possible outliers of the data set, *i.e.*, spectra, which differ notably from the found clusters. There can be several reasons for outliers in the data set. They can be spectra where elements from two adjacent minerals can be seen and such data points are so called local outliers, which are located between clusters in respective projection. In case of possible accessory minerals or coarse measurement errors, *e.g.*, intensive cosmic ray signal in the spectrum, the points are global outliers located outside of all clusters. To reduce the effect of these outliers we propose the following practice and spatial-median algorithm to replace outlier spectra with reasonable data. First, the mission is to find the right number of outliers and specify their reason. This can be done by alternating meta-parameters of DBSCAN and then check the result spectra. If we are only interested in global outliers, we

must find out parameters, which gives the rest of the data in one cluster and just finds global outliers. If we are also interested in local outliers, we need to cluster data set to several clusters. After a right number of outliers has been detected, Algorithm 1 can be used to replace outlier as a median spectrum from its neighborhood.

Algorithm 1:

1. Select spatial neighborhood of the outlier.
2. Compute PCA for these spectra
3. Determinate data point, from which spectrum corresponds the median of 1. principal component
4. Replace outlier with spectrum of the data point selected in 3.

For the evaluation of the results obtained by VCA and clustering methods, two alternative techniques were used in the visualization of spodumene occurrence. Firstly, a model spectrum was measured from a representative spodumene sample, and it was applied to the original data with linear fitting procedure with the constraint of negative coefficients, *i.e.*, non-negative least squares' algorithm (Lsqnonneg) from a Matlab toolbox. The principles of fitting are described in more detail elsewhere, *e.g.*, (53) and use of this method in mineral identification has been demonstrated in sulfide-bearing samples from the massive pyrite-copper-zinc Pyhäsalmi deposit with LIBS (54). Secondly, as the lithium content is at the highest in spodumene, relative lithium distributions are visualized as intensity maps. In this data set, lithium is detected in all minerals, most likely related to LIBS sensitivity to Li analysis and the line intensities remain rather low outside the spodumene regions. A cut-off level for representing spodumene was therefore experimentally selected to show only the locations, where the intensity value was over 60 % of the maximum value of integral of the Li line.

Data analysis was carried out with Python 3.7 and Mathworks Matlab R2015a programs. Image manipulations were made with Inkscape 0.91 and GIMP 2.8.16. As the Maps 1 and 2 were both measured from sample 1, the data sets were combined, but visualization and analysis were carried out separately.

3. Results & discussion

3.1 Development of the statistical approaches with rich spectral data

The photograph of two measured areas from Li-pegmatite rock sample (Maps 1 and 2) is shown in Fig. 2. The orientation of the greenish spodumene grains can be observed in the enlarged photos, especially in those illuminated with 248 nm laser light, where spodumene has red luminescence.
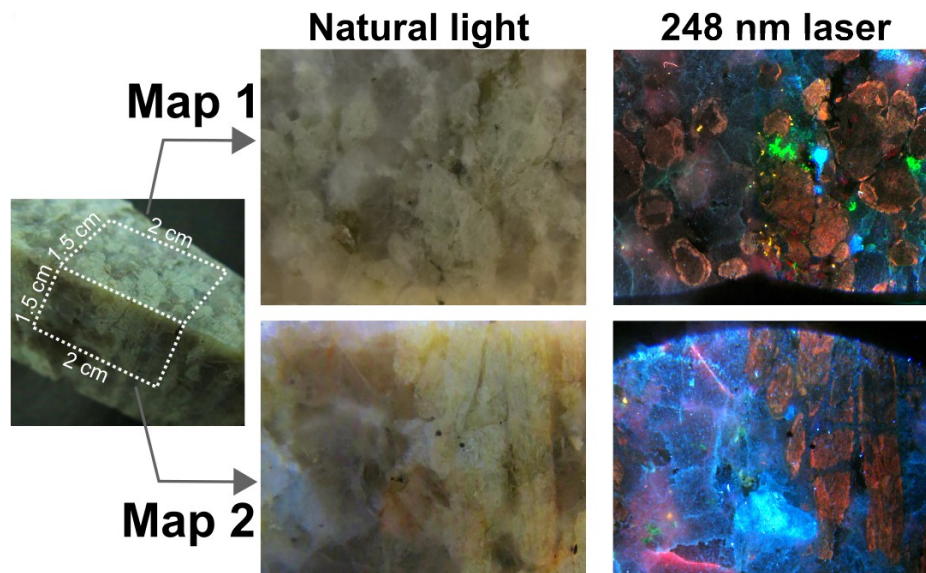

Figure 2. Photographs of Maps 1 and 2 under natural and laser light visualize the character of the sampled areas. Two perpendicular surfaces were measured to ensure that orientation of spodumene grains, which in this sample show orange luminescence, does not have significant influence on the results of data analysis.

For the development of statistical data analysis, data set with rich spectral information, *i.e.*, spectra measured at wide spectral range to provide multiple emission lines, was used. In total, the combined data set of Maps 1 and 2 contained 3800 spectra showing emission lines from 280 nm to 820 nm with 18233 pixels per spectrum (Table 3). In the first step of the procedure presented in Fig. 1, a combination of PCA and DBSCAN was applied to the data set. Optimal results in the determination of clusters were obtained when the neighborhood was set to 4000 and a minimum of three neighbors and six principal components were used. With this approach, the six PCs explained the main characters of the spectral data set. Of these PCs 1–3 explain the main mineralogical characters while PCs 4–6 represent mostly

geochemical alterations. With PCA, we reduced data set to $\mathbb{R}^6$ and the first three reduced PCs explained 90.37 % of singular values. As a result of DBSCAN, 14 outliers were found and replaced, and their features are further discussed in Section 3.3. The spectral analysis was continued with the determination of the main minerals by grouping the spectra with VCA and two clustering algorithms, DBSCAN and K-means.

3.1.1. Spectral unmixing with VCA

Linear spectral unmixing method, vertex component analysis (VCA), found five spectral endmembers, *i.e.*, prototype spectra, groups from the data sets of Maps 1 and 2. The VCA maps (Fig. 3) visualize the location of the data points as proportion maps, which express into what extent the spectrum on each point can be explained by the prototype spectra, as described in Section 2.3. The endmembers are supposed to present the prototype spectra of the main minerals and the main elements are marked in the spectra (Fig. 3, middle).
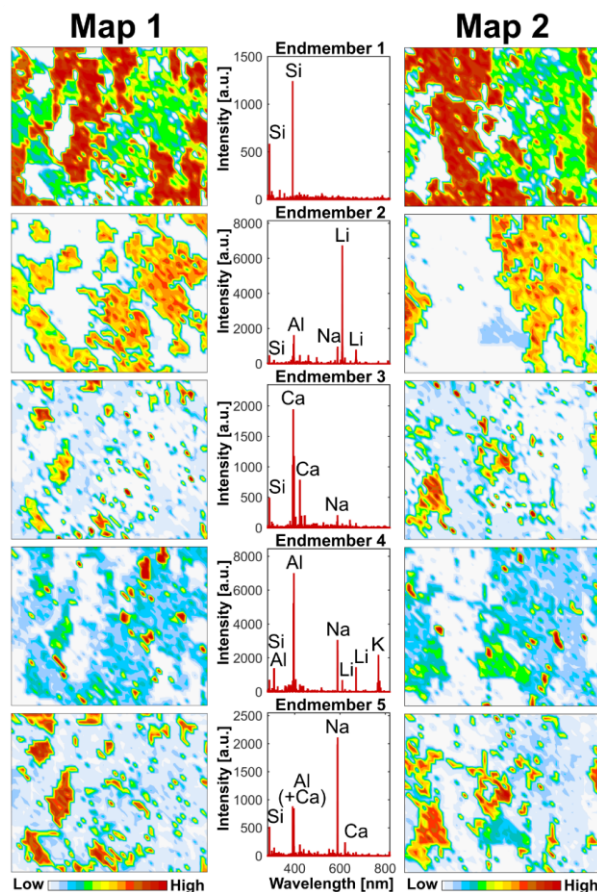

Figure 3. The five endmembers of vertex component analysis (VCA) represent the main minerals in Maps 1 and 2 and the characteristic elements are marked in the endmember spectra. It is assumed that the whole data set can be interpret as a linear combination of endmembers prototype, *i.e.*, spectra. The constructed maps illustrate the proportions, how much the spectrum at the certain data point is explained by respective endmember.

Only silicon emission lines can be seen in endmember 1 and the most intense regions in the respective maps represent chemically the simplest quartz form and these correspond to macroscopically recognized minerals seen in Fig. 2. Because the main minerals of spodumene pegmatites are silicates (Table 1), endmember 1 shows correlation (green) to other mineral regions as well. In endmember 2 spectrum, major lines are lithium, silicon, aluminum, and sodium, and it can be mainly seen to represent spodumene as the lithium emission line intensity is the highest. When the VCA map of endmember 2 is compared to the photo under UV laser light (Fig. 2), clear correlation to the location of luminescent spodumene grains can be detected. Endmember 3 spectrum shows lines of silicon, calcium, and sodium, and the highest occurrence in the maps is connected to a few small locations with high calcium content in the original spectra. Endmember 4 spectrum has the lines of aluminum, silicon, sodium, lithium, and potassium, which are typical for K-bearing minerals: K-feldspar and muscovite (Table 1). From endmember 5 lines of silicon, aluminum, calcium, and sodium can be detected and the chemical composition correlates to albite (Table 1). To verify the result that endmember 2 is representing spodumene locations, maps based on the Lsqnonneg fitting of spodumene model spectrum and intensity distribution of Li emission line 812.6 nm were constructed (Section 2.3). Constructed maps and the estimated spodumene percentages can be compared with VCA maps of endmember 2 (Fig. 4).
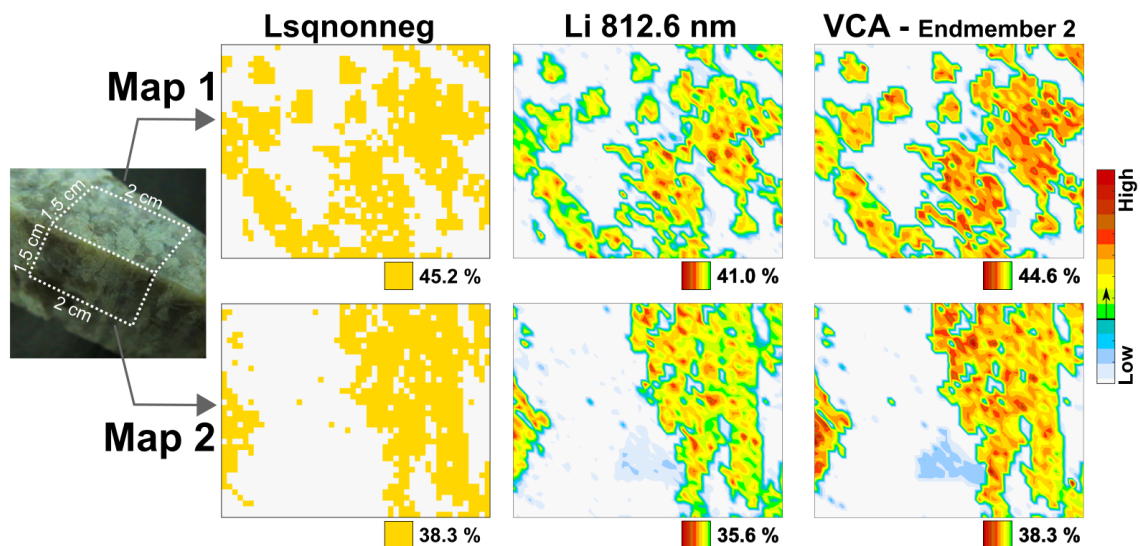

Figure 4. A comparison of three methods for the identification of the spodumene occurrence: a model spectrum matching using Lsqnonneg fitting (left), lithium distribution with integral of line 812.6 nm (middle), and maps of VCA endmember 2 (right).

The spatial occurrence of spodumene determined by VCA correlates to the maps from the alternative approaches. The percentage values of spodumene contents in the sampled area,

12

calculated from the most probable locations visualized in Fig. 4, are similar. In the maps, where the results are based on the mineral recognition (Lsqnonneg and VCA) instead of elemental content, slightly higher values were obtained. The difference is most likely caused by the classification of spectra at the borders of the spodumene grains. The laser can also hit another mineral simultaneously, *e.g.*, quartz, resulting in lower lithium intensity value, but the mineral classification can count the mixture still as spodumene group. The interpretation is supported by the observation, that the highest lithium content (Fig. 4. middle) seems to be decreasing towards the edges of spodumene grains. In general, the results are comparable, and no remarkable difference can be detected between the surfaces related to measurement on surfaces parallel either perpendicular to the spodumenes' longest crystal axes. Therefore, the pegmatite samples can be measured regardless orientation of the spodumene grains. It can be noted that a triangle-shaped area in Map 2 can be observed in endmembers 2, 4, and 5 in VCA maps which corresponds to intense blue luminescence in Fig. 2. In the closer look to the original LIBS spectra from this area, we found lines of beryllium (313.0 nm and 332.1 nm), indicating the presence of beryl ($Be_3Al_2Si_6O_{18}$), which can be found as an accessory mineral in the Kaustinen Li-pegmatites (55). These spectra were found similar to the spectra reported in LIBS research of beryl (33). It seems, that the appearance of two beryllium lines, is not enough to separate the beryl to its own group. Beryl spectra contain also rather intensive lithium lines, as demonstrated the light blue area in the Li distribution map (Fig. 4, middle).

3.1.2. Cluster analyses with K-means and DBSCAN

Two cluster analyses (K-means and DBSCAN) were carried out with the pre-reduced spectral data set of the Maps 1 and 2. K-means, using three principal components, divided the data into six clusters based on the distance from the cluster center. Centroid spectra and the corresponding maps of clusters are presented in Fig. 5. Projection of all six clusters with respect to the first three reduced principal components is also presented.
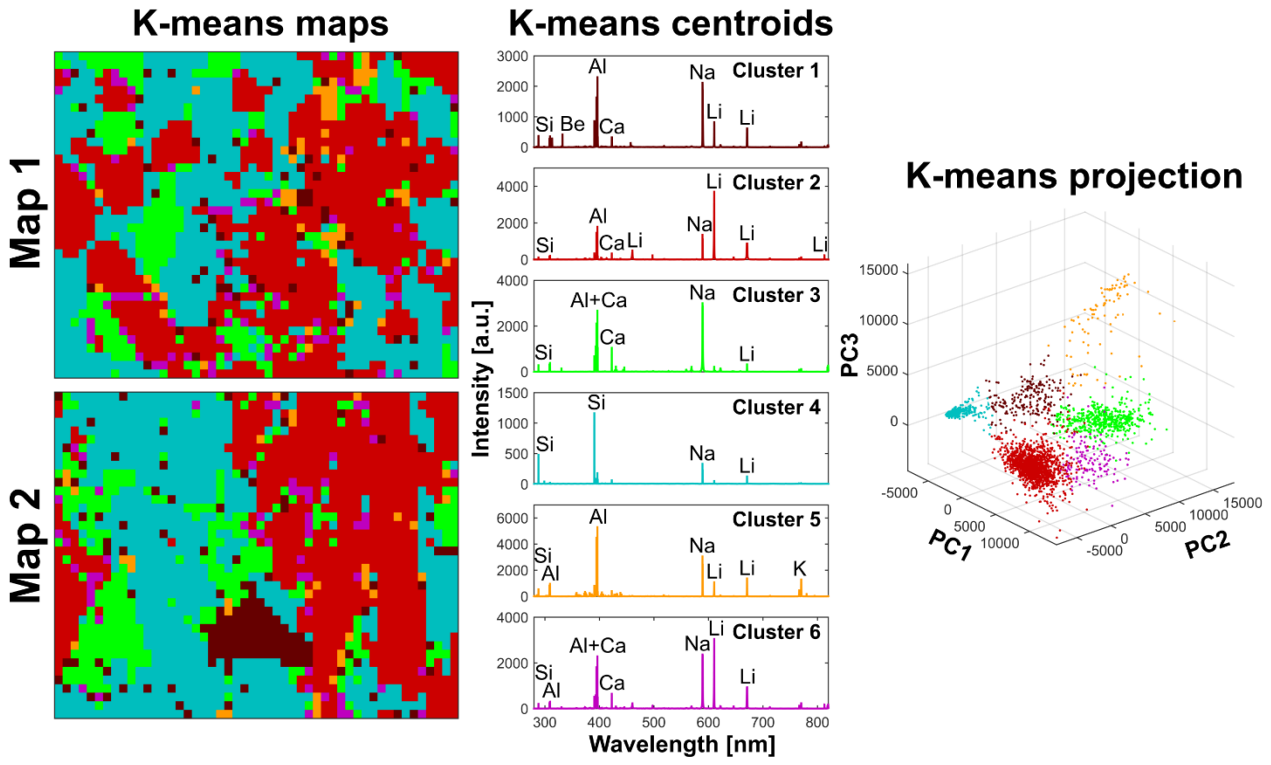
Figure 5. K-means cluster analysis presented as maps (left), corresponding cluster centroid spectra (middle), and cluster projection (right).

The interpretation of the K-means centroids is based on the appearance of the major spectral lines which have been marked to the respective spectra. Five of these were found to be presenting the minerals of Li-pegmatites: beryl (cluster 1, brown), spodumene (cluster 2, red), albite (cluster 3, green), quartz (cluster 4, turquoise), and K-feldspar/muscovite (cluster 5, orange). Because the centroid is a mean spectrum from all the spectra within the cluster, also lines from the trace elements are observed. Some remarks can be made from the projection of clusters. The red points (spodumene) appear very densely together, so clustering is efficient at the separation of spodumene from the other minerals. Other clearly separated ones are green (albite), and turquoise (quartz). In the projection the brown (beryl) and orange (K-feldspar/muscovite) points are more separated. The centroid of cluster 1 was interpreted as beryl, as it contains beryllium lines. The respective projection is somewhat separated and, also few spectra of some other mineral were found to be clustered into this. In case of orange cluster (K-feldspar/muscovite) separation of projection is explained by the cluster consisting of more than one chemically rather similar mineral, which both may also have of chemical variations. The projection of cluster 6 (violet) is located between the clusters of spodumene and albite and the centroid spectrum clearly contains lines originating

from both minerals. Thus, this cluster is composed most likely from spectra formed when the laser beam is hitting these minerals simultaneously at their borders.

In another cluster analysis, DBSCAN, the neighborhood size for the reduced data set was determined to be 1000 and a minimum number of neighbors to 30. Four cluster groups were formed and DBSCAN maps, corresponding centroid spectra and the data projected with the first three reduced principal components are presented in Fig. 6.
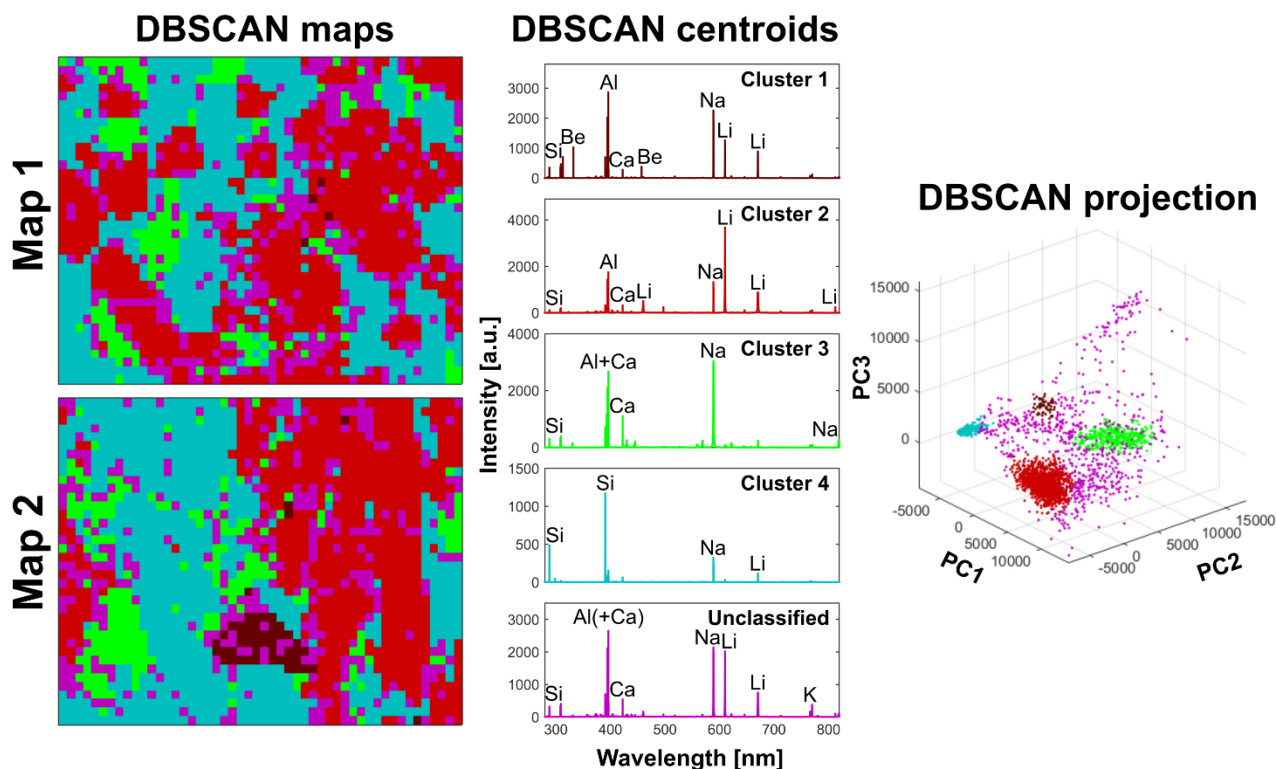

Figure 6. DBSCAN cluster analysis presented as maps (left), corresponding cluster centroid spectra (middle), and cluster projection (right).

The centroid spectra of DBSCAN analysis were interpret as the following mineralogical groups: beryl (cluster 1, brown), spodumene (cluster 2, red), albite (cluster 3, green), and quartz (cluster 4, turquoise). The rest of the data, which are not grouped in DBSCAN are presenting unclassified spectra (violet). The centroid spectra (Fig. 6, middle) show several elements. Potassium in the centroid spectrum indicates that the K-bearing minerals, K-feldspar/muscovite, are also included in this group of unclassified spectra. The projection of the DBSCAN data shows that four clusters are occurring as individual groups, while the violet points representing the unclassified data are dispersed all around the projection. When the centroid spectra of DBSCAN (Fig. 6) are compared with the ones generated by K-means

for clusters 1–4 (Fig. 5), only slight differences are observed mainly at the appearance of small lines, *i.e.*, trace elements.

The percentage levels of recognized minerals from K-means and DBSCAN analyses were calculated from the maps and are presented in Table 4. DBSCAN has somewhat lower levels in all minerals and a rather high amount of data (19 %) are left as unclassified spectra (violet, Fig. 6). It can be estimated that spodumene group in DBSCAN contains fewer intermediate spectra than K-means. Higher levels of spodumene are achieved with K-means, and the numbers are comparable to the results obtained from the spodumene recognition based on Li distribution (Fig. 4, Map 1: 41.0 % & Map 2: 35.6 %).

Table 4. Percentages of minerals recognized from the spectral data of Maps 1 and 2 with K-means and DBSCAN.

Mineral	Map 1		Map 2	
	K-means (%)	DBSCAN (%)	K-means (%)	DBSCAN (%)
Spodumene	41.0	36.5	35.5	31.5
Quartz	35.8	34.5	38.2	37.5
Albite	12.9	9.7	14.0	10.8
K-feldspar/Muscovite	2.9	–	1.8	–
Beryl	3.3	0.2	7.4	2.7
Combination	4.1		3.1	
Unclassified		19.1		17.5

3.2 Feasibility for VCA, K-means, and DBSCAN in spodumene recognition with a limited spectral information

In the second part of the study, we tested how developed statistical approaches work, if the spectral range is limited to show only the most informative spectral lines to the characterization of spodumene. These measurements were performed with a Czerny-Turner type spectrometer, because within the grating the orders of the spectral lines can overlap. The spectral range (560–815 nm) shows intensive lithium lines at 610.4, 670.8 nm, and 812.6 nm, but also potassium at 766.5 and 769.9 nm, and sodium at 589.3 as well as at 568.7 nm can be detected. We can also observe second order emission lines of aluminum at 616.4 and 618.6 nm, and silicon at 576.3 nm (Fig. 7).
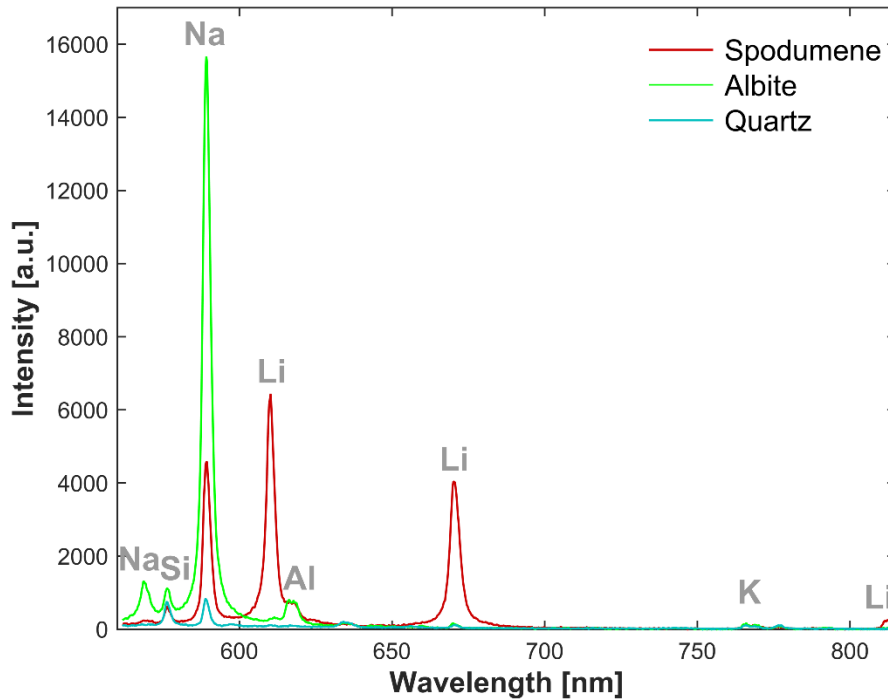
Figure 7. Limited spectral range measurements from spodumene, albite, and quartz with marked lines, of which Si and Al are 2nd order.

The outliers were first determined with combination PCA and DBSCAN from data set of Maps 3–5 (Table 3). Altogether 30 outliers were detected: 12 from the Map 3, 16 from the Map 4, and two from the Map 5. Most of the mineralogical characteristics were explained with three PCs and each of the data sets was reduced to $\mathbb{R}^3$. Singular values for three reduced PCs explained 99.8 % for Map 3, 99.4 % for Map 4, and 99.4 % for Map 5.

When a limited spectral range was used, in VCA three endmembers from each of the Maps were formed, and they were recognized as spodumene, albite, and quartz. As the focus was on the detection of the main ore mineral, the endmembers recognized as spodumene are visualized as maps (Fig. 8) together with respective photos and spodumene locations determined by Lsqnonneg as well as lithium intensity distribution. On the contrary to the map in Fig. 4, here the intensity of the line 610.4 nm was used to demonstrate the spodumene occurrence, because the 812.6 nm line intensity was small due to the lower efficiency of both grating and ICCD at 800 nm range (Fig. 8). Line 610.4 nm was more suitable for the task than resonance line 670.8 nm which suffers from self-absorption. For VCA, the lesser number of the spectral lines measured does not seem to influence the determination of spodumene content, if the characteristic lines of the main minerals can be observed. The

grain size and the spodumene content is significantly smaller in Map 5 and macroscopically investigation is challenging. However, with VCA there is no notable effect on the calculated percentages between three data analysis approaches.

It can be remarked that opposite to the luminescence behavior of spodumene observed in Fig. 2, within these samples the spodumene grains are not showing uniform luminescence under UV laser light irradiation (Fig 8, left). However, in Map 5 spodumene seems to occur with red luminescence in UV light (Fig. 8), which enables to estimating the length of the spodumene grains as 1 mm at the highest. It can be also noted, that spodumene grains in Map 3 have reddish color in natural light, which is common to spodumene from the Läntta deposit.
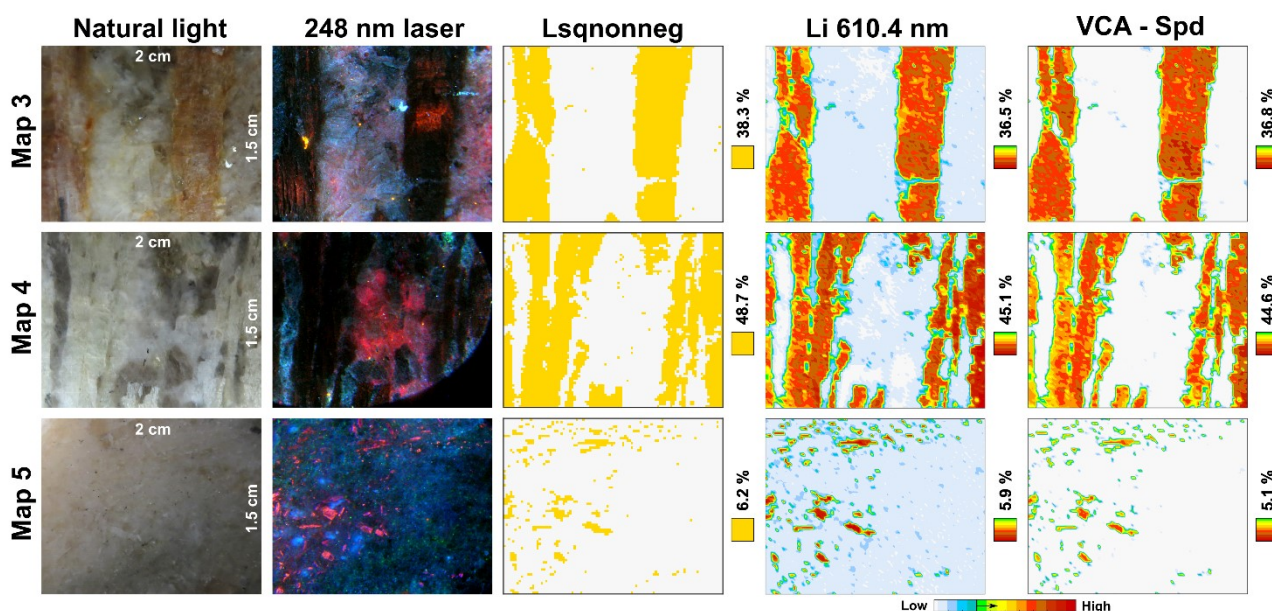

Figure 8. The capability of VCA in the detection of spodumene in the case of optimized spectral range is tested against Lsqnonneg fitting of the model spectrum and spatial lithium intensity distribution. The dissimilarity of three Li-pegmatites can be seen in photographs under natural and laser light.

The K-means and DBSCAN cluster analyses were carried out separately to the data of Maps 3–5. The visualization of the clustering maps and their projections are demonstrated in Fig. 9. In K-means procedure, from the data of Maps 3 and 4 was formed three clusters while from data of Map 5 was formed only two. The parameters for the DBSCAN were the same as in for the data of Maps 1 and 2 and as a result, DBSCAN found four clusters for Map 3, three clusters for Map 4, and two clusters for Map 5.
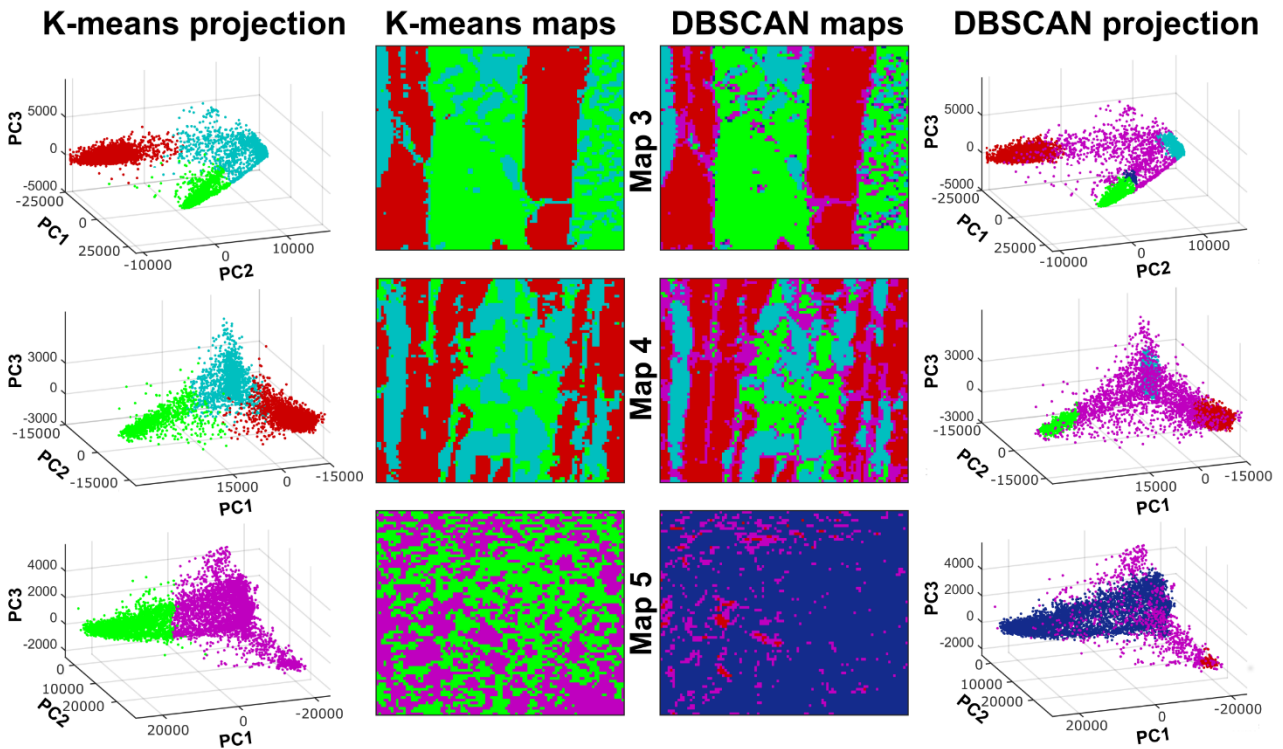
Figure 9. K-means and DBSCAN analyses for Maps 3, 4, and 5.

It is obvious, that the clusterings are not as efficient when the spectral information is cut down from the range of 280–820 nm (~18 000 pixels) to 560–815 nm (~1 000 pixels). Nevertheless, in the centroid spectra of the coarse- and medium-grained samples (Maps 3 and 4) the mean spectrum with the highest lithium intensity can be characterized as spodumene and can be used to separate other silicate minerals. In the K-means projections in Fig. 9, the respective cluster is illustrated with red color and within the projections of Maps 3 and 4, the red cluster seems to be separated from blue and green clusters without notable spatial variations. The calculated spodumene percentages (Map 3: 35.8 %; Map 4: 43.0 %) for K-means are quite comparable with results gained with VCA and alternative techniques in Fig. 8. The results from the DBSCAN spodumene detection were similar but the percentages of spodumene were 33.4 % for Map 3 and 35.4 % for Map 4. It seems, that with the data of limited spectral information, DBSCAN gives somewhat lower spodumene percentage values, in general, than the other methods presented in Table 5, especially at the medium-grained and fine-grained samples (data of Maps 4 & 5). The reason for this is most likely due to the fact, that on the contrary to other methods, DBSCAN clustering lefts some spectra as unclassified. In the closer look we noticed that these spectra locate in

19

mineral grain borders in the respective maps and most likely represent the intermediate spectra of two minerals. In the coarse-grained sample (Map 3) the number of unclassified spectra is thus smaller and the spodumene percentage is closer to the ones obtained by other methods.

When considering the data of the fine-grained sample with low spodumene content (Map 5), K-means seems to fail in the detection of the cluster with features of spodumene. DBSCAN is somewhat more effective: the data of Map 5 can be separated into spodumene (red: 1.4 %) and to group, which centroid interpreted as intermediate spectra of albite and quartz (blue, 87.6 %). The recognition was based on the relative intensities of lines of Na, Al, and Si in the blue centroid. The rest of the data of Map 5 was not grouped with DBSCAN (violet: 11.0 %) and it most likely contains also spectra measured from spodumene grain edges, as the centroid contained rather high lithium intensities. Spodumene contents obtained with different data analysis procedures of Maps 3, 4, and 5 are collected into Table 5.

Table 5. The spodumene content (%) estimated by VCA, DBSCAN, and K-means for the coarse-grained (Map 3), medium-grained (Map 4) and fine-grained (Map 5) Li-pegmatite samples. For comparison, percentages from the Lsqnonneg fitting of the model spectrum and spatial lithium intensity distribution, visualized in Fig. 8, are also given.

	Map 3 (%)	Map 4 (%)	Map 5 (%)
VCA spd	36.8	44.6	5.1
DBSCAN	33.4	35.4	1.4
K-means	35.8	43.0	–
Lsqnonneg	38.3	48.7	6.2
Lithium level	36.5	45.1	5.9

3.3 Outliers in detection of accessory minerals

Altogether 14 global outliers, *i.e.*, spectra, which differ notably from found clusters, were distinguished from the spectral data of Maps 1 and 2, as described in Section 3.1. Although the global outliers were removed from the data set before the main data analysis, the closer inspection of their spectra can give insight to accessory minerals. Two of them were found to be an intermediate spectrum of three main minerals: spodumene, albite, and K-feldspar/muscovite, while the rest of the outliers are calcium and niobium rich minerals. The representative spectrum of the calcium rich mineral (Fig. 10. a) include only several strong calcium emission lines. Because this spectral range does not allow detection phosphorus or carbon, this could be either spectrum of apatite or calcite, both known to occur accessory

minerals in the target area (23). The Nb-rich mineral spectrum (Fig. 10. b) represents most likely Nb-Ta oxide which has also been recognized in the Kaustinen lithium pegmatite province (23). This is also supported by the fact, that the spectrum (Fig. 10. b) matches to the previous results of Ta-Nb ores analyzed with LIBS (56).
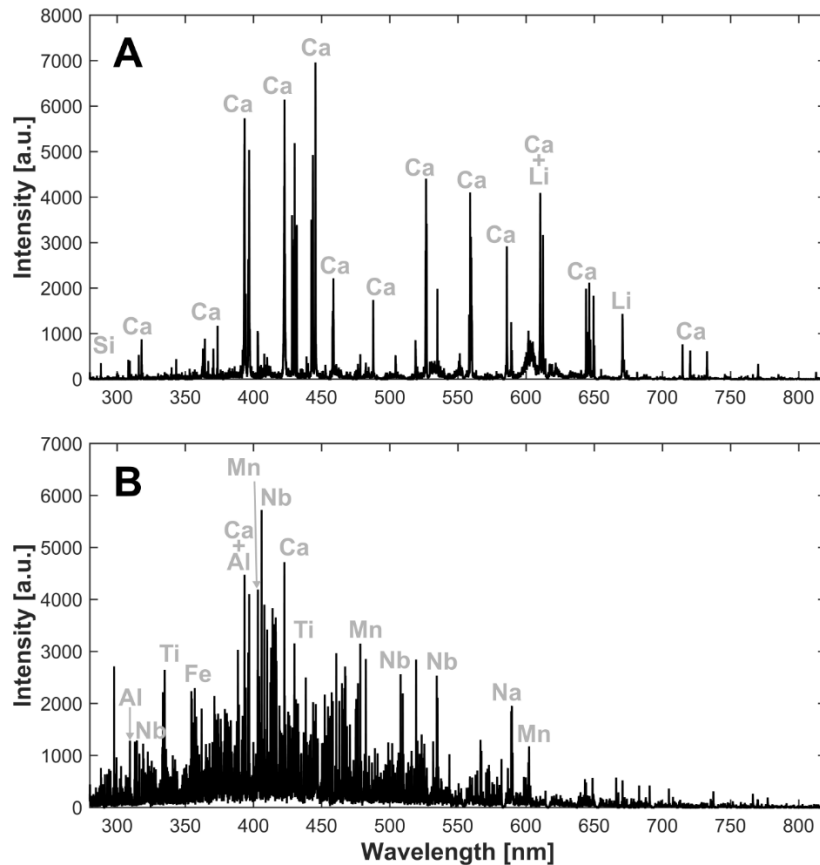

Figure 10. Examples of spectra recognized as outliers from Maps 1 and 2.

In limited spectral range measurements (Maps 3–5) in total 30 outliers were detected. Because this range contained only a few elemental peaks (see Fig. 7), it was not possible to perform thorough accessory mineral analysis. In general, outlier detection can be a valuable tool for achieving information about the location and composition of accessory minerals.

4. Conclusions

We utilized laser-induced breakdown spectroscopy (LIBS) with sophisticated statistical methods in analysis of Li-pegmatite ore samples. Key factors in the research were that no beforehand knowledge of the mineralogy was needed, and the size of spectral data was

optimized. Vertex component analysis (VCA) and two cluster analyses (K-means and DBSCAN) were used to separate the ore mineral spodumene from the gangue, estimate its content and visualize texture. VCA was able to separate spodumene regardless the mineral grain size. Both clustering analyses found spodumene in coarse- and medium-grained samples, but the information about the other main minerals was lost when the spectral information was limited to lines of the main minerals. The presented approaches may serve as a basis for *in-situ* and online applications also in analysis of other Li-bearing minerals.

5 Acknowledgements

6 References

1. European Commission. (2020) *Study on the review of the list of Critical Raw Materials - Final Report*.

2. U.S. Geological Survey. (2020) Lithium. In *Mineral Commodity Summaries 2020*, U.S. Geological Survey: Reston, pp 98–99.

3. Tadesse, B., Makuei, F., Albijanic, B., and Dyer, L. (2019) The beneficiation of lithium minerals from hard rock ores: A review. *Miner. Eng.* 131: 170–184.

4. Rasilainen, K., Eilu, P., Ahtola, T., Halkoaho, T., Kärkkäinen, N., Kuusela, J., Lintinen, P., and Törmänen, T. (2018) *Quantitative assessment of undiscovered resources in lithium-caesium-tantalum pegmatite-hosted deposits in Finland*.

5. Gourcerol, B., Gloaguen, E., Melleton, J., Tuduri, J., and Galiegue, X. (2019) Re-assessing the European lithium resource potential – A review of hard-rock resources and metallogeny. *Ore Geol. Rev.* 109: 494–519.

6. Butcher, A. (2010) A practical Guide to Some Aspects of Mineralogy that Affect Flotation. In *Flotation Plant Optimisation*, pp 83–93.

7. Cremers, D. A., and Chinni, R. C. (2009) Laser-induced breakdown spectroscopy-capabilities and limitations. *Appl. Spectrosc. Rev.* 44 (6): 457–506.

8. Song, K., Lee, Y. I., and Sneddon, J. (1997) Applications of laser-induced breakdown spectrometry. *Appl. Spectrosc. Rev.* 32 (3): 183–235.

9. Fernandes Andrade, D., Pereira-Filho, E. R., and Amarasiriwardena, D. (2021) Current trends in laser-induced breakdown spectroscopy: a tutorial review. *Appl. Spectrosc. Rev.* 56 (2): 98–114.

10. Qiao, S., Ding, Y., Tian, D., Yao, L., and Yang, G. (2015) A review of laser-induced breakdown spectroscopy for analysis of geological materials. *Appl. Spectrosc. Rev.* 50 (1): 1–26.

11. Harmon, R. S., Remus, J., McMillan, N. J., McManus, C., Collins, L., Gottfried, J. L., DeLucia, F. C., and Miziolek, A. W. (2009) LIBS analysis of geomaterials: Geochemical fingerprinting for the rapid analysis and discrimination of minerals. *Appl. Geochemistry* 24 (6): 1125–1141.

12. Harmon, R. S., Lawley, C. J. M., Watts, J., Harraden, C. L., Somers, A. M., and Hark, R. R. (2019) Laser-induced breakdown spectroscopy-An emerging analytical tool for mineral exploration. *Minerals* 9 (12): 1–45.

13. Li, W., Li, X., Li, X., Hao, Z., Lu, Y., and Zeng, X. (2020) A review of remote laser-induced breakdown spectroscopy. *Appl. Spectrosc. Rev.* 55 (1): 1–25.

14. Rakovský, J., Musset, O., Buoncristiani, J., Bichet, V., Monna, F., Neige, P., and Veis, P. (2012) Testing a portable laser-induced breakdown spectroscopy system on geological samples. *Spectrochim. Acta - Part B At. Spectrosc.* 74–75: 57–65.

15. Lawley, C. J. M., Somers, A. M., and Kjarsgaard, B. A. (2021) Rapid geochemical imaging of rocks and minerals with handheld laser induced breakdown spectroscopy (LIBS). *J. Geochemical Explor.* 222: 106694.

16. Fabre, C., Boiron, M. C., Dubessy, J., Chabiron, A., Charoy, B., and Martin Crespo, T. (2002) Advances in lithium analysis in solids by means of laser-induced breakdown spectroscopy: An exploratory study. *Geochim. Cosmochim. Acta* 66 (8): 1401–1407.

17. Rossi, M., Dell'Aglio, M., De Giacomo, A., Gaudiuso, R., Senesi, G. S., De Pascale, O., Capitelli, F., Nestola, F., and Ghiara, M. R. (2014) Multi-methodological investigation of kunzite, hiddenite, alexandrite, elbaite and topaz, based on laser-induced breakdown spectroscopy and conventional analytical techniques for supporting mineralogical characterization. *Phys. Chem. Miner.* 41 (2): 127–140.

18. Sweetapple, M. T., and Tassios, S. (2015) Laser-induced breakdown spectroscopy (LIBS) as a tool for in situ mapping and textural interpretation of lithium in pegmatite minerals. *Am. Mineral.* 100 (10): 2141–2151.

19. Verlaguet, A., Brunet, F., Goffé, B., Menut, D., Findling, N., Poinssot, C., and Huet, B. (2016) Selective transfer of Li-Al-rich phyllosilicate to metamorphic veins (Western Alps): Laser Induced Breakdown Spectroscopy (LIBS) compositional profiles and microstructural characterization. *J. Geodyn.* 101: 51–72.

20. Stipe, C. B., Miller, A. L., Brown, J., Guevara, E., and Cauda, E. (2012) Evaluation of laser-induced breakdown spectroscopy (LIBS) for measurement of silica on filter samples of coal dust. *Appl. Spectrosc.* 66 (11): 1286–1293.

21. Cremers, D. A., and Radziemski, L. J. (2013) *Handbook of laser-induced breakdown spectroscopy*. 2nd ed. John Wiley & Sons, Ltd: Chichester, West Sussex, U.K.

22. Weast, R. C. (1974) *CRC Handbook of Chemistry & Physics*. 56th ed. CRC Press Inc.: Cleveland, Ohio.

23. Ahtola, T., Kuusela, J., Käpyaho, A., and Kontoniemi, O. (2015) *Overview of lithium pegmatite exploration in the Kaustinen area in 2003-2012*.

24. Kuusela, J., Ahtola, T., Koistinen, E., Seppänen, H., Hatakka, T., and Lohva, J. (2011) *Report of investigations on the Rapasaaret lithium pegmatite deposit in Kaustinen-Kokkola, Western Finland*.

25. Sweco Industry Oy. (2016) *Pre-feasibility Study: Keliber Lithium Project*.

26. Deer, W. A., Howie, R. A., and Zussman, J. (2013) An Introduction to the Rock-Forming Minerals., Mineralogical Society of Great Britain and Ireland.3rd ed.

27. Ataide Salvador, D. (2017) Geometallurgical Variability Study of Spodumene Pegmatite Ores, Central Ostrobothnia - Finland.

28. Piñon, V., Mateo, M. P., and Nicolas, G. (2013) Laser-induced breakdown spectroscopy for chemical mapping of materials. *Appl. Spectrosc. Rev.* 48 (5): 357–383.

29. Zhang, D., Zhang, H., Zhao, Y., Chen, Y., Ke, C., Xu, T., and He, Y. (2020) A brief review of new data analysis methods of laser-induced breakdown spectroscopy: machine learning. *Appl. Spectrosc. Rev.*

30. Alvey, D. C., Morton, K., Harmon, R. S., Gottfried, J. L., Remus, J. J., Collins, L. M., and Wise, M. A. (2010) Laser-induced breakdown spectroscopy-based geochemical fingerprinting for the rapid analysis and discrimination of minerals: The example of garnet. *Appl. Opt.* 49 (13): C168–C180.

31. Death, D. L., Cunningham, A. P., and Pollard, L. J. (2009) Multi-element and mineralogical analysis of mineral ores using laser induced breakdown spectroscopy and chemometric analysis. *Spectrochim. Acta - Part B At. Spectrosc.* 64 (10): 1048–1058.

32. Klus, J., Mikysek, P., Prochazka, D., Pořízka, P., Prochazková, P., Novotný, J., Trojek, T., Novotný, K., Slobodník, M., and Kaiser, J. (2016) Multivariate approach to the chemical mapping of uranium in sandstone-hosted uranium ores analyzed using double pulse Laser-Induced Breakdown Spectroscopy. *Spectrochim. Acta - Part B At. Spectrosc.* 123: 143–149.

33. McManus, C. E., McMillan, N. J., Harmon, R. S., Whitmore, R. C., De Lucia, F. C., and Miziolek, A. W. (2008) Use of laser induced breakdown spectroscopy in the determination of gem provenance: Beryls. *Appl. Opt.* 47 (31).

34. Gottfried, J. L., Harmon, R. S., De Lucia, F. C., and Miziolek, A. W. (2009) Multivariate analysis of laser-induced breakdown spectroscopy chemical signatures for geomaterial classification. *Spectrochim. Acta - Part B At. Spectrosc.* 64 (10): 1009–1019.

35. Clegg, S. M., Sklute, E., Dyar, M. D., Barefield, J. E., and Wiens, R. C. (2009) Multivariate analysis of remote laser-induced breakdown spectroscopy spectra using partial least squares, principal component analysis, and related techniques. *Spectrochim. Acta - Part B At. Spectrosc.* 64 (1): 79–88.

36. Ytsma, C. R., Knudson, C. A., Dyar, M. D., McAdam, A. C., Michaud, D. D., and Rollosson, L. M. (2020) Accuracies and detection limits of major, minor, and trace element quantification in rocks by portable laser-induced breakdown spectroscopy. *Spectrochim. Acta - Part B At. Spectrosc.* 171: 105946.

37. Hark, R. R., Remus, J. J., East, L. J., Harmon, R. S., Wise, M. A., Tansi, B. M., Shughrue, K. M., Dunsin, K. S., and Liu, C. (2012) Geographical analysis of 'conflict minerals' utilizing laser-induced breakdown spectroscopy. *Spectrochim. Acta - Part B At. Spectrosc.* 74–75: 131–136.

38. Ollila, A. M., Lasue, J., Newsom, H. E., Multari, R. A., Wiens, R. C., and Clegg, S. M. (2012) Comparison of two partial least squares-discriminant analysis algorithms for identifying geological samples with the ChemCam laser-induced breakdown spectroscopy instrument. *Appl. Opt.* 51 (7): B130–B142.

39. Zhu, X., Xu, T., Lin, Q., Liang, L., Niu, G., Lai, H., Xu, M., Wang, X., Li, H., and Duan, Y. (2014) Advanced statistical analysis of laser-induced breakdown spectroscopy data to discriminate sedimentary rocks based on Czerny-Turner and Echelle spectrometers. *Spectrochim. Acta - Part B At. Spectrosc.* 93: 8–13.

40. Guo, Y. M., Guo, L. B., Hao, Z. Q., Tang, Y., Ma, S. X., Zeng, Q. D., Tang, S. S., Li, X. Y., Lu, Y. F., and Zeng, X. Y. (2018) Accuracy improvement of iron ore analysis using laser-induced breakdown spectroscopy with a hybrid sparse partial least squares and least-squares support vector machine model. *J. Anal. At. Spectrom.* 33 (8): 1330–1335.

41. Anderson, R. B., Bell, J. F., Wiens, R. C., Morris, R. V., and Clegg, S. M. (2012) Clustering and training set selection methods for improving the accuracy of quantitative laser induced breakdown spectroscopy. *Spectrochim. Acta - Part B At. Spectrosc.* 70: 24–32.

42. Müller, S., Meima, J. A., and Rammlmair, D. (2021) Detecting REE-rich areas in heterogeneous drill cores from Storkwitz using LIBS and a combination of k-means clustering and spatial raster analysis. *J. Geochemical Explor.* 221: 106697.

43. Yang, Y., Hao, X., Zhang, L., and Ren, L. (2020) Application of scikit and keras libraries for the classification of iron ore data acquired by laser-induced breakdown spectroscopy (LIBS). *Sensors (Switzerland)* 20 (5): 1393.

44. Romppanen, S., Häkkänen, H., and Kaski, S. (2017) Singular value decomposition approach to the yttrium occurrence in mineral maps of rare earth element ores using laser-induced breakdown spectroscopy. *Spectrochim. Acta - Part B At. Spectrosc.* 134: 69–74.

45. Chen, J., Pisonero, J., Chen, S., Wang, X., Fan, Q., and Duan, Y. (2020) Convolutional neural network as a novel classification approach for laser-induced breakdown spectroscopy applications in lithological recognition. *Spectrochim. Acta - Part B At. Spectrosc.* 166: 105801.

46. Meima, J. A., and Rammlmair, D. (2020) Investigation of compositional variations in chromitite ore with imaging Laser Induced Breakdown Spectroscopy and Spectral Angle Mapper classification algorithm. *Chem. Geol.* 532: 119376.

47. Sheng, L., Zhang, T., Niu, G., Wang, K., Tang, H., Duan, Y., and Li, H. (2015) Classification of iron ores by laser-induced breakdown spectroscopy (LIBS) combined with random forest (RF). *J. Anal. At. Spectrom.* 30 (2): 453–458.

48. Nascimento, J. M. P., and Dias, J. M. B. (2005) Vertex component analysis: A fast algorithm to unmix hyperspectral data. *IEEE Trans. Geosci. Remote Sens.* 43 (4): 898–910.

49. Boardman, J. W., Kruse, F. A., and Green, R. O. (1995) Mapping Target Signatures Via Partial Unmixing of Aviris Data. *Summ. Fifth JPL Airborne Earth Sci. Work. Pasadena, 23-26 January 1995*: 95–101.

50. Bioucas-Dias, J. M., Plaza, A., Member, S., Dobigeon, N., Parente, M., Du, Q., Gader, P., Chanussot, J., and Bioucas-Dias, J. M. (2012) Hyperspectral Unmixing Overview:

Geometrical, Statistical, and Sparse Regression-Based Approaches. *IEEE J. Sel. Top. Appl. Earth Obs. Remote Sens.* 5 (2): 354–379.

51.   MacQueen, J. (1967) Some methods for classification and analysis of multivariate observations. *Proc. fifth Berkeley Symp. Math. Stat. Probab.* 1 (233): 281–296.

52.   Ester, M., Kriegel, H.-P., Sander, J., and Xu, X. (1996) A Density-Based Algorithm for Discovering Clusters in Large Spatial Databases with Noise. *Proc. 2nd Int. Conf. Knowl. Discov. Data Min.*: 226–231.

53.   Lawson, C. L., and Hanson, R. J. (1995) Linear least squares with linear inequality constraints. In *Solving Least Squares Problems*, pp 158–173.

54.   Kaski, S., Häkkänen, H., and Korppi-Tommola, J. (2003) Sulfide mineral identification using laser-induced plasma spectroscopy. *Miner. Eng.* 16 (11 SUPPL.): 1239–1243.

55.   Al-ani, T., and Ahtola, T. (2008) *Mineralogy of spodumene pegmatites, Western Finland*. Available at: http://tupa.gtk.fi/raportti/arkisto/m19_2323_2008_61.pdf.

56.   Liu, L., and Hao, Z. (2019) Quantitative determination of tantalum and niobium in tantalum–niobium ore using laser-induced breakdown spectroscopy. *Appl. Opt.* 58 (2): 461.